

Published in final edited form as:

*Magn Reson Med.* 2011 February ; 65(2): 471–479. doi:10.1002/mrm.22556.

## Determination of whole-brain oxygen extraction fractions by fast measurement of blood T<sub>2</sub> in the jugular vein

Qin Qin<sup>1,2</sup>, Ksenija Grgac<sup>1,2,3</sup>, and Peter C. M. van Zijl<sup>1,2</sup>

<sup>1</sup> The Russell H. Morgan Department of Radiology and Radiological Science, Division of MR Research, The Johns Hopkins University School of Medicine, Baltimore, MD USA

<sup>2</sup> F. M. Kirby Center for Functional Brain Imaging, Kennedy Krieger Institute, Baltimore, MD USA

<sup>3</sup> Department of Chemistry, The Johns Hopkins University, MD USA

### Abstract

The oxygen extraction fraction (OEF) of the brain reports on the balance between oxygen delivery and consumption and can be used to assess deviations in physiological homeostasis. This is relevant clinically as well as for calibrating BOLD fMRI responses. OEF is reflected in the arteriovenous difference in oxygen saturation fraction ( $Y_v - Y_a$ ), which can be determined from venous T<sub>2</sub> values when arterial oxygenation is known. A pulse sequence is presented that allows rapid measurement (< 1 min) of blood T<sub>2</sub>s in the internal jugular vein. The technique combines slice-saturation and blood inflow to attain high signal to noise ratio in blood and minimal contamination from tissue. The sequence is sensitized to T<sub>2</sub> using a non-selective Carr-Purcell-Meiboom-Gill (CPMG) T<sub>2</sub> preparation directly after slice saturation. Fast scanning (TR of about 2 s) is possible by using a non-selective saturation directly after acquisition to rapidly achieve steady-state longitudinal magnetization. The venous T<sub>2</sub> (for 10 ms CPMG inter-echo time) for normal volunteers was  $62.4 \pm 6.1$  ms ( $n = 20$ ). A calibration curve relating T<sub>2</sub> to blood oxygenation was established using a blood perfusion phantom. Using this calibration, a whole-brain OEF of  $0.37 \pm 0.04$  was determined ( $n = 20$ ), in excellent agreement with literature values.

### Keywords

*in vivo* blood T<sub>2</sub>; CPMG; oxygen extraction fraction; OEF; internal jugular vein

### Introduction

The oxygen extraction fraction (OEF) of the brain reports on the balance between oxygen delivery and consumption (1). Slight changes in OEF may reflect physiological perturbation, and a method to rapidly and noninvasively assess this parameter should be useful for clinical assessment of brain homeostasis. In addition, the BOLD functional MRI effect reflects focal changes in OEF during activation (2–4), and changes in baseline OEF will affect the size of the BOLD effect. Measurement of whole-brain OEF would therefore be useful to calibrate the BOLD effect for baseline blood oxygenation in a manner similar to Lu et al. (5). The OEF is defined as (1,6):

$$OEF = \frac{\text{oxygen consumption}}{\text{oxygen delivery}} = \frac{CMRO_2}{C_a \cdot CBF} = \frac{CMRO_2}{[Hb_{tot}] \cdot Y_a \cdot CBF} \quad [1]$$

in which  $CMRO_2$  is the cerebral metabolic rate for oxygen and  $C_a$  the oxygen content, the product of total hemoglobin concentration  $[Hb_{tot}]$  in mM and the arterial oxygen saturation fraction ( $Y_a$ ). CBF is the cerebral blood flow.

The venous deoxygenation fraction ( $1 - Y_v$ ) is directly related to OEF via the modified Kety equation accounting for hypoxia (3)

$$1 - Y_v = 1 - Y_a + OEF \cdot Y_a \quad [2]$$

The blood deoxygenation fraction ( $1 - Y$ ) in any type of vessel is directly related to  $1/T_2$  in that vessel (7–12) and calibration curves relating these two parameters can be used to determine  $Y$ -values from absolute  $T_2$  (13–17). Determination of the venous relaxation times  $T_{2,v}$ , would allow determination of the oxygenation fractions of blood in these vessels, and, if  $Y_a$  is known (or assumed) and a calibration curve available, the subsequent calculation of OEF.

Measurement of blood  $T_2$  *in vivo* is challenging because of the rapid flow of blood in larger vessels and the small size of microvascular blood vessels. To avoid the wash-in/wash-out effect encountered in conventional spin-echo sequences for large blood vessels, magnetization-prepared  $T_2$  weightings ( $T_2$  prep) are typically employed before image acquisition (18). Flow-insensitive  $T_2$  prep uses only non-selective (NS) RF pulses and consists of a train of refocusing pulses bracketed by an excitation pulse and a flip-back pulse with a total duration  $TE_{prep}$  (18). This was first used to measure coronary venous blood  $T_2$  a decade ago (14). Recently, this approach was extended to determine  $T_2$  in the sagittal sinus (19). In that study, the complication of partial volume effects with tissue around the sagittal sinus was reduced by using the difference between the control and the spin labeled (on venous side) scans (19). This spin-tagging technique took about 5 minutes due to the long TR (8 s) needed to wait for equilibrium and the use of a control/label pair for subtraction.

Jugular venous blood primarily drains the cerebral hemispheres (usually 97%, minimally 93% of the intracranial circulation system) (20) and is a favorable sample source to estimate whole-brain OEF. In this work, we present a pulse sequence that allows rapid measurement (48 s) of jugular blood  $T_2$ s by exploiting the fact that the internal jugular vein (IJV) has faster flow and a bigger cross-sectional area than the sagittal sinus. In order to determine venous oxygenation ( $Y_v$ ) and thus OEF from the measured  $T_2$  value, a calibration curve relating  $T_2$  and  $Y$  at different hematocrit (Hct) and oxygenation levels ( $Y$ ) was measured *in vitro* using a blood circulation system.

## Methods

### Pulse Sequence for *In Vivo* Blood $T_2$ Measurement

All experiments were performed on a 3T Philips Achieva scanner (Philips Medical Systems, Best, The Netherlands). *In vivo* experiments used the body coil for transmission (maximum RF amplitude 575 Hz) and an 8-channel head coil for reception. The pulse sequence diagram for measuring blood  $T_2$  in the jugular vein is shown in Figure 1a. It includes 4 blocks within each TR: slice-selective (SS) saturation, non-selective (NS)  $T_2$  prep, SS excitation/acquisition and NS saturation. The NS  $T_2$  prep block starts with a hard pulse excitation

( $90^\circ_x$ , 0.44 ms), followed by a series of composite refocusing pulses ( $90^\circ_x 180^\circ_y 90^\circ_x$ , pulse width (pw) = 1.75 ms) with an MLEV phase pattern (21), and then a flip-back pulse ( $270^\circ_x 360^\circ_{-x}$ , 3.05 ms), which was made composite to compensate for RF field ( $B_1$ ) inhomogeneity (18).

In order to generate a preparation sequence with multiple echo times,  $TE_{\text{prep}} = [20, 40, 80, 160]$  ms, and constant inter-echo spacing of  $\tau_{\text{CPMG}} = 10$  ms, the number of refocusing pulses,  $k$ , was chosen to be 2, 4, 8, and 16, respectively (19). The necessity to use composite pulses to accomplish reliable refocusing *in vivo* and the limit of the RF amplitude of the body coil within a human scanner resulted in a RF pulse fraction of almost 18% of the refocusing interval. Using the theory in (22), it can be calculated that this will lead to almost 9% overestimation (Eq. [2] of (22):  $\Delta T_2/T_2 \approx (1/2) (pw/\tau_{\text{CPMG}}) = (1/2) \cdot (1.75/10) \approx 8.8\%$ ) of the measured  $T_2$ , due to the slower  $T_1$  decay of the temporarily stored longitudinal magnetizations during the composite pulses. The corrected echo times without  $T_1$  influence can be calculated based on Eq. [3] of (22):  $TE_{\text{prep,corr}} = TE - k \cdot (pw/2) \cdot (1 - T_{2,v}/T_{1,v}) = [18.3, 36.6, 73.2, 146.5]$  ms, assuming  $T_{2,v} = 60$  ms and  $T_{1,v} = 1800$  ms (23). These  $TE_{\text{prep,corr}}$  values are insensitive to different relaxation time ratios of blood ( $T_1/T_2$  between 10 to 40). At the end of the  $T_2$  prep block, the longitudinal magnetizations of both static tissue and flowing blood are weighted by their  $T_2$  factor,  $\exp(-TE_{\text{prep,corr}}/T_2)$ . The residual transverse magnetizations are dephased by a spoiling gradient after the last tip-up pulse (18).

After SS excitation (THK = 5 mm), linear-order flow compensation (FC) gradients, and data acquisition with following spoiling gradients, a NS adiabatic saturation pulse (BIR-4 (24), of length 10 ms, and bandwidth 400 Hz) immediately resets all remaining longitudinal magnetization to zero. As a consequence, after a fixed time delay,  $T_{\text{delay}}$ , the longitudinal magnetization of the blood right before the next  $T_2$  prep block is proportional only to  $1 - \exp(-T_{\text{delay}}/T_1)$ . By using the same pre-delay time ( $T_{\text{delay}}$ ) between global saturation and the next scan, the same steady-state will be achieved before each  $T_2$  prep block, independent of the length of the preparation and the previous  $T_2$  weighting history (14,18).

When using the sequence above, tissue can obscure the blood signals, because tissue magnetization also experiences  $T_2$  weighting and its  $T_2$  is on the order of 60 ~ 90 ms at 3T, comparable to venous blood  $T_2$  at  $\tau_{\text{CPMG}} = 10$  ms. Given that blood velocity ( $v$ ) of healthy volunteers is in the range of 5~40 cm/s in the IJV (25), a SS saturation pulse applied on the same image slice is performed at  $T_{\text{sat}} = 200$  ms before the SS excitation. This  $T_{\text{sat}}$  is short enough to saturate the static tissue signal and yet long enough to replenish the flowing spins in the imaging slice ( $T_{\text{sat}} > \text{THK}/v$ ). Even with the reported slowest velocity  $v = 5$  cm/s in the IJV,  $T_{\text{sat}} = 200$  ms is still twice the time for complete replacement of blood in an imaging slice of thickness (THK) 5 mm.

### **In Vivo Data acquisition**

A total of 20 healthy volunteers (age:  $39 \pm 13$  yrs; range: 24–63 yrs; 10 females and 10 males) were enrolled for parameter optimization and determination of blood  $T_2$ , all of whom provided informed written consent in accordance with local IRB guidelines.

As part of scan planning, phase-contrast MRA (PCA) survey images were acquired in both coronal and sagittal planes to visualize the location and orientation of IJVs and internal carotid arteries (ICAs). PCA survey scans used a 50 mm slab, TR/TE = 20/5.8 ms, FOV =  $250 \times 250$  mm<sup>2</sup>, and a scan matrix of  $256 \times 128$  (acquisition time: 20 s for 2 averages). Phase-contrast velocity measurements for IJVs were performed on a 5 mm axial slice, positioned perpendicular to the targeted IJV about 15 mm below the superior bulb (Figure 1b, c, d). The encoding velocity was set to be 40 cm/s. Acquisition parameters: TR/TE = 15/9 ms, 5 dynamics, FOV =  $128 \times 128$  mm<sup>2</sup>, acquisition matrix =  $128 \times 128$

(reconstruction  $256 \times 256$ ). The total acquisition duration for velocity measurement was about 30 sec.

The blood  $T_2$  measurements were performed at the same location as the blood velocity measurement. Acquisition parameters were: FOV =  $200 \times 150 \text{ mm}^2$ , acquisition matrix =  $192 \times 132$ , with left-right being the phase encoding direction. Data were zero-filled to  $0.78 \times 0.78 \text{ mm}^2$  in-plane resolution. In order to minimize image distortion and signal loss,  $k$ -space was acquired with a 6-segment gradient echo EPI ( $N_{\text{shots}} = 6$ ), with SENSE acceleration factor = 2, resulting in a minimum TE of 15 ms.  $T_{\text{delay}} = 2 \text{ s}$  was used for most of the measurements, which led to a total  $T_2$  measurement time  $\approx 2 \text{ s} (T_{\text{delay}}) \times 6 (N_{\text{shots}}) \times 4 (N_{\text{TEprep}}) = 48 \text{ s}$ .

A SS pre-saturation block was added to minimize the stationary tissue signals but not perturb the  $T_2$  weighting of the flowing blood. To illustrate its effect, data were acquired for five subjects with and without the SS saturation block. Both images and fitted  $T_2$ s from blood vessels were compared.

Since the NS  $T_2$  prep and NS saturation block both aim for blood covered within the body transmit coil (brain + neck) before it flows through the IJV and because the RF pulses have limited bandwidth, it is important to properly shim on the whole volume within the transmit coil, in addition to the local imaging slice. Therefore, as suggested from our blood  $T_1$  study (23), only 1<sup>st</sup> order shims were adjusted locally following a global shim in order not to affect the shimming around the neck area to an extent that the field there is outside the bandwidth. The effect of NS saturation block was therefore examined for different areas of the brain (top, middle, and bottom) by using the same BIR-4 pulse right before SS excitation/acquisition, while keeping the shimming conditions used in blood  $T_2$  measurements.

Effects of different  $T_{\text{delay}}$  were evaluated on five volunteers, with the expectation that longer  $T_{\text{delay}}$  should only increase the signal-to-noise ratio at the cost of longer scan duration, but not change the measured blood  $T_2$ s.  $T_{\text{delay}}$  values of 2, 3, 4, 5, and 6 s were used, corresponding to a total acquisition duration of about 1, 1.5, 2, 2.5, and 3 min, respectively, while all other imaging parameters were kept the same. Some subjects (three of them) have left and right IJVs similar in orientation and sizes so they were also chosen to inspect the correspondence of measured blood  $T_2$ s from the two vessels. The same  $T_2$  results were confirmed from the left and right IJVs of the same subject (data not shown).

Subjects in all studies were instructed to stay awake during the scans, which was checked frequently, to avoid potential baseline oxygenation changes during sleep.

### **In Vitro Experiments**

Calibration curves relating transverse relaxation times and oxygenation ( $Y = 0.35 \sim 1.0$ ) were measured for bovine blood over a range of physiologically relevant hematocrit (Hct) values (0.36, 0.40, 0.46, 0.50). Blood was circulated in a gas exchange perfusion system at controlled physiological temperature ( $37^\circ\text{C}$ ) within the 3T magnet. Details of the blood preparation and the perfusion system setup were described previously (26). Once a stable  $Y$  value is achieved within a mixing chamber, bovine blood is pumped into a circulation loop, and maintained at a speed about 1 cm/s through a 1 cm-diameter, 10 cm-long, vertically positioned sample tube for the relaxation time measurements. Blood was sampled right before and after the MR measurements and oxygenation determined using a blood gas analyzer (Radiometer, ABL700) to ensure less than 3% difference of  $Y$ . In addition, blood  $p\text{O}_2$  was monitored during the MR measurement with a needle-encased sensor (Oxford Optrox) placed close to the tube.

*In vitro* blood studies were conducted with the same 3T magnet as the *in vivo* scans, but a quadrature head coil was used for both transmission (maximum RF amplitude 851 Hz) and reception. *In vitro* blood  $T_2$  measurements utilized a sequence similar to the one described in Figure 1a, but without the SS saturation block before the  $T_2$  prep, because this SS saturation approach is only suited for fast flowing blood and there is no need to suppress static tissues in the phantom. Within the  $T_2$  prep block, hard pulses were used for  $90^\circ$  and  $180^\circ$  pulses with durations 0.3 ms and 0.6 ms respectively and the CPMG phase pattern was applied, similar to other work in the field (27,28). Imperfect refocusing pulses will lead to undesired signal loss. So a water phantom (with  $T_2 \approx 2$  s) was first scanned to confirm proper  $180^\circ$  pulses (data not shown), which were easy to attain over the small sample volume. Using  $\tau_{\text{CPMG}} = 10$  ms,  $T_2$  was measured using six equally-spaced  $TE_{\text{prep}}$ s ranging from 20 to 120 ms. After SS excitation (THK = 10 mm), a single-shot gradient-echo EPI was employed for acquisition (FOV =  $64 \times 64$  mm<sup>2</sup>,  $32 \times 32$  acquisition matrix, TE = 11 ms).  $T_{\text{delay}} = 3$  s was fixed between the NS saturation after acquisition and the following  $T_2$  prep block for all of the *in vitro* blood  $T_2$  measurements. The total measurement time was  $3 \text{ s} (T_{\text{delay}}) \times 1 (N_{\text{shots}}) \times 6 (N_{TE_{\text{prep}}}) \approx 18$  s for each specific Y and Hct value.

### Data Analysis

Matlab 7.0 (MathWorks, Inc., Natick, MA, USA) was used for data processing. Since the surrounding tissue signals were suppressed, regions of interest (ROIs) at IJVs could be easily drawn manually on the images acquired at  $TE_{\text{prep}} = 20$  ms. Blood  $T_2$  for each pixel was fitted using a linear-least-square algorithm for the monoexponential signal decay curve. For *in vivo* data, the shortened  $TE_{\text{prep,corr}}$  for composite refocusing pulses was used; while the original  $TE_{\text{prep}}$  for hard  $180^\circ$  pulses was used *in vitro*. For individual measurements, the standard error of the estimated  $T_2$ s fitted from ROI-based mean values are reported. For a group of measurements, the mean and standard deviation (std) of the averaged  $T_2$ s over all subjects were calculated.

Extensive literature exists on studying the dependence of blood  $T_2$  on Y, Hct and  $\tau_{\text{CPMG}}$  (3,9,12,16,27–30). To explain the exact mechanisms underlying the measured effects, both an exchange model between plasma and erythrocyte (30) and a diffusion model with weak magnetic inhomogeneities (29) have been postulated. Our *in vitro* blood  $T_2$  values obtained at 3T are still being analyzed to further elucidate this topic. However, exact knowledge of the mechanistic relationship between  $1/T_2$  and  $(1-Y)$  is not needed to measure a calibration curve. Therefore, the curves between  $T_2$  and Y were fitted similar to the literature, namely as an empirical quadratic equation, which approximates the experimental data very well:

$$1/T_2 = A + C(1 - Y)^2 \quad [3]$$

The fitted calibration curve at Hct = 0.40 was used to convert the blood  $T_2$  measured *in vivo* to corresponding oxygen saturation fraction levels Y. Subsequently, OEF was estimated from:

$$\text{OEF} = (Y_a - Y_v) / Y_a \quad [4]$$

with  $Y_a$  assumed to be 0.98 (5). Because typical physiological Hct values range between 0.36 and 0.50, errors for estimating Y and OEF by using a calibration curve at a fixed Hct = 0.40 were also assessed.

## Results

### *In Vitro* Experiments

In Figure 2a, the transverse relaxation rates ( $1/T_2$ ) of bovine blood at  $\tau_{\text{CPMG}} = 10$  ms are shown as a function of oxygen saturation fraction for four different hematocrits. The data clearly conform to linearity with respect to the square of deoxygenation level,  $(1-Y)^2$ , as described by Eq. [3]. The fitted parameters A and C for each condition as well as the calculated  $T_2$  for a venous oxygenation level of 0.61 are summarized in Table 1.

For the purpose of estimating Y from our *in vivo* blood  $T_2$  measurements, the average constants of fitted results at Hct = 0.40 and 0.46 ( $A = 7.18$ ,  $C = 59.6$ ) were used. It can be seen from both Figure 2b and Table 1 that at a  $\tau_{\text{CPMG}}$  of 10 ms, Hct = 0.40 and Hct = 0.46 have almost identical relationship between  $T_2$  and Y over a broad range of possible venous Y values. The dependency of  $T_2$  on Hct reduces with decreasing oxygenation, which is helpful for the accuracy of our estimates. For the range of  $T_2$  values between 54 and 72 ms measured in the jugular vein in our study (reported below), Y estimated using the calibration curve at assumed Hct range between 0.40 and 0.46 will cause an overestimation of only about 4.4% for true Hct = 0.36 and an underestimation of about 6.0% for true Hct = 0.50. These will be the limits of the estimation errors of Y for the venous blood since most physiological Hct values are within this range.

### *In Vivo* Experiments

In order to assess whether all blood is refreshed after the SS saturation, we first measured blood velocities in most subjects ( $n = 13$ ). Average blood velocities in the IJVs were  $15 \pm 6$  cm/s, with a range of 5~21 cm/s ( $n = 13$ ). These are all fast enough (limit  $v > 5$  cm/s) for the proposed SS saturation not to affect the blood  $T_2$  measurements. The effect of the SS pre-saturation block is demonstrated in Figure 3, where an image collected without saturation (Figure 3a,b) is compared to one with saturation (Figure 3d,e). Tissue signals were reduced significantly when using SS saturation, allowing easier selection of vascular ROIs. However, no significant difference was observed between the  $T_2$  curves without (Figure 3c) and with SS saturation (Figure 3f), providing validation for this approach.

In order to test the effectiveness of the post-acquisition NS saturation, we performed  $T_2$  measurements as a function of  $T_{\text{delay}}$ . The results in Figure 4 confirm that there is negligible effect of  $T_{\text{delay}}$ , based on which we used  $T_{\text{delay}} = 2$  s, allowing data acquisition in a period of 48 s. One disadvantage of using a short pre-delay is a reduction in SNR, but based on the measured standard deviation, this is not yet an issue when using  $T_{\text{delay}} = 2$  s.

The individual blood  $T_2$  values from the IJV for all twenty volunteers are listed in Table 2. No significant differences in  $T_2$  values (two-tailed Student  $t$ -test:  $P = 0.48$ ) were observed between female subjects ( $T_{2, \text{IJV}} = 63.4 \pm 7.0$  ms,  $n = 10$ ) and male subjects ( $T_{2, \text{IJV}} = 61.4 \pm 5.3$  ms,  $n = 10$ ). Since  $T_2$  of fully oxygenated blood depends strongly on Hct (Figure 2), it was found not reliable to estimate  $Y_a$  from  $T_{2, \text{ICA}}$ . We therefore assumed the reasonable value of  $Y_a = 0.98$  for healthy subjects to calculate OEF from Eq. [4]. The averaged blood  $T_2$  among the 20 healthy volunteers was  $T_{2, \text{IJV}} = 62.4 \pm 6.1$  ms, corresponding to  $Y_v = 0.61 \pm 0.03$  and  $\text{OEF} = 0.37 \pm 0.04$ . When  $Y_a = 0.96$  or 1.0 are taken instead, OEF values of  $0.36 \pm 0.04$  and  $0.39 \pm 0.03$  are found, respectively.

## Discussion

A new approach for rapidly measuring blood  $T_2$  in the major neck vessels and consequent determination of whole-brain OEF using a blood  $T_2$  calibration as a function of oxygen saturation fraction is presented. The MRI measurement combines a  $T_2$  prep sequence for

blood  $T_2$  measurement (14,18,19) and a pre-preparation slice-selective saturation pulse for reducing surrounding tissue signals. It was shown that the latter does not interfere with the  $T_2$ -weighting of the blood flowing into the slice. A non-selective saturation pulse right after image acquisition resets the longitudinal magnetization of the blood independent of the previous  $T_2$  weighting pulses (14), which made the method more efficient than just waiting for its full longitudinal recovery (19).

### ***In Vitro* Calibration Experiments**

$T_2$  values of blood are often converted to the blood oxygen saturation fractions (Y) using *in vitro*  $T_2$  - Y calibration curves, which can be obtained either directly from human blood samples of the individuals studied (13,14) or indirectly from fresh animal blood (16,19) with comparable erythrocyte shape and physiological properties. Since the transverse relaxation time depends on the magnetic field and the field dependence has not been well characterized, previous work done at 1.5T (13,16,28) cannot be used reliably for  $T_2$  calibration at 3T, and we therefore measured a calibration curve for this paper. The new calibration data are of comparable order of magnitude to those of a recent characterization of *in vitro* human blood  $T_2$  at 3T as a function of Y and  $\tau_{\text{CPMG}}$  that were fitted with a diffusion model (27). Based on results from Table 1 and Eq. [4] in that paper, we calculated a calibration curve at  $\tau_{\text{CPMG}} = 10$  ms, giving  $A = 6.91$  and  $C = 44.4$ . Compared to our results ( $A = 7.18$  and  $C = 59.6$ ), these smaller calibration variables correspond with higher  $T_2$ s at the same Y values, and would lead to an underestimation of oxygenation levels by about 10~15% for the range of  $T_2$  values between 54 and 72 ms. In order to better judge this small difference, it is important to realize that these calibration curves were acquired under different conditions. First, as can be seen in the Results/*in vitro* blood section, lower Hct would cause higher  $T_2$ . Our calibration curve is an average of Hct at 0.40 and 0.46, while the other study averaged over a range of Hct from 0.35 to 0.53 (27) for 10 subjects. Since the individual data were not presented, we cannot judge the origin of potential differences. Second, our experiment was conducted at physiologic temperature as opposed to room temperature in (27). However, lower temperature should increase relaxation slightly, which can not explain the higher  $T_2$  values obtained by Chen et al. Third, bovine blood instead of human blood was used in this study. Based on literature evidence (31), the physiologic and physical properties of erythrocytes in higher mammals are very similar, and no significant difference in transverse relaxation is expected. More importantly, we used hard refocusing pulses in the  $T_2$  prep, while Chen et al. used composite  $180^\circ$  pulses, which would overestimate  $T_2$  by 9% as demonstrated in Methods/Pulse Sequence section. The first and last issues, in our assessment, resulted in the difference between the two studies.

### ***In Vivo* Experiments**

The signal decay as a function of echo time ( $TE_{\text{prep,corr}}$  in this work) should be governed by the blood water protons experiencing relaxation during transverse evolution of magnetization. The mechanism of such relaxation is quite complex, and includes chemical exchange of water molecules between plasma and erythrocytes and/or diffusion through intra/extracellular magnetic gradients (3,7-9,12,29,32). As a consequence, the relaxation time measured depends on the inter-echo spacing  $\tau_{\text{CPMG}}$ . Here we report blood  $T_2$  at  $\tau_{\text{CPMG}} = 10$  ms, to be comparable to a recent study in the sagittal sinus (19). Similar to this earlier paper, the length of the refocusing pulses was not negligible. Since this lengthens the measured relaxation time due to partial  $T_1$  decay during the composite pulses (22),  $TE_{\text{prep,corr}}$  is used for *in vivo*  $T_2$  fitting, which, in our case, reduced the effective  $\tau_{\text{CPMG}}$  to 9.15 ms. We used an *in vitro* calibration curve at  $\tau_{\text{CPMG}} = 10$  ms. This could lead to some slight underestimation of  $T_2$  (less than 3%, as estimated based on the measured relaxation time at 10 ms), and we have neglected this small difference.

The *in vivo* blood  $T_2$  measurements may have another source of irreversible dephasing of the signal from flowing through the inhomogeneous magnetic field. During half of the 10 ms interecho time, blood flows about 0.75 mm in IJVs (in average,  $v = 15$  cm/s, from this study) and up to 4 mm in ICAs ( $v < 1$  m/s, (33)). The shimming employed in this study (global shim followed by local 1<sup>st</sup> order linear shim) should minimize this external magnetic field inhomogeneity effect for IJVs, and less optimized for ICAs. As shown from the results (Figure 3, Table 1), the  $T_2$  values measured in jugular veins were more robust than in carotids. The same effect was also reported in an earlier work (13). Careful shimming is a necessity to avoid irreversible dephasing of blood signals due to fast flowing between long interecho times.

At 3T and higher fields,  $B_1$  inhomogeneity reduces pulse efficiency and complicates the measurement of relaxation rates through incorrect refocusing. To counteract these challenges, we used composite refocusing pulses with MLEV phase pattern for  $T_2$  prep (18,21) and a BIR-4 pulse (24) for NS saturation. Reproducible  $T_2$  measurements could be obtained in the IJV (Figure 3, Table 1). In principle, in addition to the stronger Y-dependence for  $T_2$  in arteries, the less stable ICA results can also be due to the more nonuniform  $B_1$  experienced by blood. For instance, when using 160 ms  $T_2$  prep, the first pulse may be experienced by blood at the edge of the body coil range, while the last one may be 15 cm higher, where  $B_1$  could be different. However, this is expected to be a small effect when using body coils for excitation. If a head-only transmit coil, instead of the body coil, were to be used in this work, the effect on jugular  $T_2$  measurement remains to be seen, but this problem is expected to be much worse for carotid  $T_2$  measurement. To address this problem, another set of composite pulses were used in (14) and adiabatic pulses were suggested in (34). However, longer pulses length and higher power deposition are associated with these alternative pulses.

### OEF Estimation

When assuming  $Y_a = 0.98$  for our normal subjects, and combining the blood  $T_2$  measurements in the jugular vein with our calibration curve obtained from *in vitro* blood  $T_2$  measurements, a whole-brain OEF value of  $0.37 \pm 0.04$  (range: 0.32–0.42,  $n = 20$ ) was found (Table 2). This is in excellent agreement with literature values (Table 3) obtained from catheterization (35), PET (36–38) and MRI (15,16,19,39–41). Compared to other modalities, MRI has the advantage of being noninvasive, but different MR techniques have different acquisition schemes and results may vary with methodology or the location of the measurement. For instance, when small local draining veins are the desired ROIs (16), high resolution images need to be acquired to avoid partial voluming with tissue or CSF and a larger number of averages is necessary to increase SNR. Even though most MRI approaches provide similar OEF results, the durations of the measurements vary. For example, in a recently published study (42) determining venous oxygenations (27) the oximetry measurement took 4.5 min. Another recently proposed promising method (40) acquired  $T_2'$  decay curves that were fitted with a sophisticated model for OEF and other parameters including deoxygenated blood volume,  $1/T_2$  of tissue and CSF volume fraction. However, this technique, which was validated for OEF measurement on a rat model (43), required a rather long acquisition time (8.5 min). Alternatively, MR susceptometry (41) was demonstrated to be useful for whole-brain OEF measurement at jugular vein. This technique records phase images to calculate susceptibility differences between blood in jugular vein and surrounding tissues. This method is also very feasible, but requires a somewhat longer acquisition time to fully characterize the background gradients from the air-tissue interface (4.3 min). In contrast, our method is based on a simple  $T_2$  model and takes only 0.8 minute for OEF measurement, making it a very suitable complementary technique for a variety of applications where a rapid whole-brain evaluation of OEF is useful.



There are some confounding factors to keep in mind when using  $T_2$  to determine blood oxygenation. As shown in Figure 2, Table 1, and other literature (9,12,32), blood  $T_2$  depends on Hct, which may affect the OEF determination. The range of Hct values for women versus men generally is: female: 0.36 ~ 0.44; male: 0.41 ~ 0.50 (44). As calculated in the Results Section and visualized in Figure 2b, use of the calibration curve for Hct values between 0.40 and 0.46 would lead to 6.7% underestimation of OEF for subjects with Hct = 0.36 and 12.4% overestimation for Hct = 0.50. So even though the measured jugular  $T_2$  values showed no significant variation between female and male groups,  $Y_v$  and OEF calibrated with a true Hct, if different, could potentially show some small difference. For instance for an average female group with lower Hct, a lower  $Y_v$  and higher OEF would be found. Therefore, caution should be exercised when employing a universal  $T_2$  - Y calibration curve, especially for subjects with hematological diseases. Similarly, for physiological conditions such as hypoxia, the arterial blood oxygen saturation,  $Y_a$ , can not be assumed to be 98%. In this case, one could use the pulse oximeter to measure  $Y_a$  from subject's fingertip to determine  $Y_a$  so that OEF can still be determined non-invasively through Eq. [4].

### Potential Applications

In recent work (5), Lu et al. have shown that the baseline venous oxygenation of individuals is inversely correlated with BOLD response and may be a substantial factor causing intersubject variations in fMRI signals. Fast measurement of this physiological parameter on each subject before or after the functional scans, would allow it to be used as a linear regressor for normalization of BOLD signals among subjects. This will be especially important for patient groups with underlying aberrant physiology.

Demonstrated by Xu et al. in a different work (17), whole-brain OEF measurements can also be used for estimation of whole-brain  $CMRO_2$ , by using the relationship in Eq. [1]. Through phase-contrast MRA, whole-brain blood flow can be quantified by assessing the velocities across ROIs on both the ICAs and vertebral arteries. Since the amount of the blood supplying the cerebral brain should equal to the amount of the draining blood, IJVs could be alternative vessels for evaluating whole-brain blood flow, with the advantage of much less pulsation effects and relatively bigger cross sections. With additional high-resolution  $T_1$  weighted images, the intracranial tissue volume can be used to normalize the total CBF to yield the unit volume CBF, which is the CBF that needs to be used in Eq. [1] when looking at whole-brain metabolism.

### Conclusions

A technique was developed to measure  $T_2$  of venous blood in the jugular vein in less than one minute, with minimum tissue contamination. In addition, a calibration curve was measured to allow determination of venous oxygenation and OEF based on the measured  $T_2$ s. This approach is expected to be useful for clinical application, e.g. to establish ischemia in patients, as well as for fast calibration of baseline OEF for BOLD experiments.

### Acknowledgments

The authors are grateful to Joseph S. Gillen, Michael Schar (Philips) for assistance in developing the pulse sequence, and Hanzhang Lu, Feng Xu for useful discussion and involvement in the blood calibration experiments. Terri Brawner, Kathleen Kahl, and Ivana Kusevic are thanked for experimental assistance. Dr. van Zijl is a paid lecturer for Philips Medical Systems. Dr. van Zijl is the inventor of technology that is licensed to Philips. This arrangement has been approved by Johns Hopkins University in accordance with its conflict of interest policies. This research was made possible in part by a grant from the National Center for Research Resources (NCRR), a component of the National Institutes of Health (NIH). Its contents are solely the responsibility of the authors and do not necessarily represent the official view of NCRR or NIH.

Grant support from

NIH-NIBIB R01-EB004130 and NIH-NCRR P41-RR15241

## References

1. Kety SS, Schmidt CF. The Effects of Altered Arterial Tensions of Carbon Dioxide and Oxygen on Cerebral Blood Flow and Cerebral Oxygen Consumption of Normal Young Men. *Journal of Clinical Investigation* 1948;27(4):484–492.
2. Ogawa S, Menon RS, Tank DW, Kim SG, Merkle H, Ellermann JM, Ugurbil K. Functional Brain Mapping by Blood Oxygenation Level-Dependent Contrast Magnetic-Resonance-Imaging - a Comparison of Signal Characteristics with a Biophysical Model. *Biophysical Journal* 1993;64(3):803–812. [PubMed: 8386018]
3. van Zijl PCM, Eleff SM, Ulatowski JA, Oja JME, Ulug AM, Traystman RJ, Kauppinen RA. Quantitative assessment of blood flow, blood volume and blood oxygenation effects in functional magnetic resonance imaging. *Nature Medicine* 1998;4(2):159–167.
4. Buxton RB, Frank LR. A model for the coupling between cerebral blood flow and oxygen metabolism during neural stimulation. *Journal of Cerebral Blood Flow and Metabolism* 1997;17(1):64–72. [PubMed: 8978388]
5. Lu HZ, Zhao CG, Ge YL, Lewis-Amezcuea K. Baseline blood oxygenation modulates response amplitude: Physiologic basis for intersubject variations in functional MRI signals. *Magnetic Resonance in Medicine* 2008;60(2):364–372. [PubMed: 18666103]
6. Siesjo BK. Cerebral-Circulation and Metabolism. *Journal of Neurosurgery* 1984;60(5):883–908. [PubMed: 6425463]
7. Meyer ME, Yu O, Eclancher B, Grucker D, Chambron J. Nmr Relaxation Rates and Blood Oxygenation Level. *Magnetic Resonance in Medicine* 1995;34(2):234–241. [PubMed: 7476083]
8. Gillis P, Peto S, Moyny F, Mispelter J, Cuenod CA. Proton Transverse Nuclear Magnetic-Relaxation in Oxidized Blood - a Numerical Approach. *Magnetic Resonance in Medicine* 1995;33(1):93–100. [PubMed: 7891542]
9. Bryant RG, Marill K, Blackmore C, Francis C. Magnetic-Relaxation in Blood and Blood-Clots. *Magnetic Resonance in Medicine* 1990;13(1):133–144. [PubMed: 2319929]
10. Gomori JM, Grossman RI, Yuip C, Asakura T. Nmr Relaxation-Times of Blood -Dependence on Field-Strength, Oxidation-State, and Cell Integrity. *Journal of Computer Assisted Tomography* 1987;11(4):684–690. [PubMed: 3597895]
11. Brooks RA, Dichiro G. Magnetic-Resonance-Imaging of Stationary Blood - a Review. *Medical Physics* 1987;14(6):903–913. [PubMed: 3696078]
12. Thulborn KR, Waterton JC, Matthews PM, Radda GK. Oxygenation Dependence of the Transverse Relaxation-Time of Water Protons in Whole-Blood at High-Field. *Biochimica Et Biophysica Acta* 1982;714(2):265–270. [PubMed: 6275909]
13. Wright GA, Hu BS, Macovski A. Estimating Oxygen-Saturation of Blood In vivo with Mr Imaging at 1.5t. *Jmri-Journal of Magnetic Resonance Imaging* 1991;1(3):275–283.
14. Foltz WD, Merchant N, Downar R, Stainsby TA, Wright GA. Coronary venous oximetry using MRI. *Magnetic Resonance in Medicine* 1999;42(5):837–848. [PubMed: 10542342]
15. Oja JME, Gillen JS, Kauppinen RA, Kraut M, van Zijl PCM. Determination of oxygen extraction ratios by magnetic resonance imaging. *Journal of Cerebral Blood Flow and Metabolism* 1999;19(12):1289–1295. [PubMed: 10598932]
16. Golay X, Silvennoinen MJ, Zhou JY, Clingman CS, Kauppinen RA, Pekar JJ, van Zijl PCM. Measurement of tissue oxygen extraction ratios from venous blood T-2: Increased precision and validation of principle. *Magnetic Resonance in Medicine* 2001;46(2):282–291. [PubMed: 11477631]
17. Xu F, Ge YL, Lu HZ. Noninvasive Quantification of Whole-Brain Cerebral Metabolic Rate of Oxygen (CMRO2) by MRI. *Magnetic Resonance in Medicine* 2009;62(1):141–148. [PubMed: 19353674]
18. Brittain JH, Hu BS, Wright GA, Meyer CH, Macovski A, Nishimura DG. Coronary Angiography with Magnetization-Prepared T-2 Contrast. *Magnetic Resonance in Medicine* 1995;33(5):689–696. [PubMed: 7596274]

19. Lu HZ, Ge YL. Quantitative evaluation of oxygenation in venous vessels using T2-Relaxation-Under-Spin-Tagging MRI. *Magnetic Resonance in Medicine* 2008;60(2):357–363. [PubMed: 18666116]
20. Purves, MJ. *The Physiology of The Cerebral Circulation*. Cambridge: University Press; 1972.
21. Levitt MH, Freeman R, Frenkiel T. Broad-Band Heteronuclear Decoupling. *Journal of Magnetic Resonance* 1982;47(2):328–330.
22. Foltz WD, Stainsby JA, Wright GA. T-2 accuracy on a whole-body imager. *Magnetic Resonance in Medicine* 1997;38(5):759–768. [PubMed: 9358450]
23. Qin Q, Van Zijl PCM. Measuring Blood T1 in the Jugular Vein: Juggling Size, Speed and Precision. *Proc Intl Soc Mag Reson Med Honolulu* 2009;17:3624.
24. Garwood M, Yong K. Symmetrical Pulses to Induce Arbitrary Flip Angles with Compensation for Rf Inhomogeneity and Resonance Offsets. *Journal of Magnetic Resonance* 1991;94(3):511–525.
25. Pucheu A, Evans J, Thomas D, Scheuble C, Pucheu M. Doppler Ultrasonography of Normal Neck Veins. *Journal of Clinical Ultrasound* 1994;22(6):367–373. [PubMed: 8071454]
26. Zhao JM, Clingman CS, Narvainen MJ, Kauppinen RA, van Zijl PCM. Oxygenation and Hematocrit dependence of transverse relaxation rates of blood at 3T. *Magnetic Resonance in Medicine* 2007;58(3):592–597. [PubMed: 17763354]
27. Chen JJ, Pike GB. Human Whole Blood T-2 Relaxometry at 3 Tesla. *Magnetic Resonance in Medicine* 2009;61(2):249–254. [PubMed: 19165880]
28. Stefanovic B, Pike GB. Human whole-blood relaxometry at 1.5T: Assessment of diffusion and exchange models. *Magnetic Resonance in Medicine* 2004;52(4):716–723. [PubMed: 15389952]
29. Jensen JH, Chandra R. NMR relaxation in tissues with weak magnetic inhomogeneities. *Magnetic Resonance in Medicine* 2000;44(1):144–156. [PubMed: 10893533]
30. Brooks RA, Moyny F, Gillis P. On T-2-shortening by weakly magnetized particles: The chemical exchange model. *Magnetic Resonance in Medicine* 2001;45(6):1014–1020. [PubMed: 11378879]
31. Benga G, Borza T. Diffusional water permeability of mammalian red blood cells. *Comparative Biochemistry and Physiology B-Biochemistry & Molecular Biology* 1995;112(4):653–659.
32. Silvennoinen MJ, Clingman CS, Golay X, Kauppinen RA, van Zijl PCM. Comparison of the dependence of blood R-2 and R\*(2) on oxygen saturation at 1.5 and 4.7 Tesla. *Magnetic Resonance in Medicine* 2003;49(1):47–60. [PubMed: 12509819]
33. Blackshear WM, Phillips DJ, Chikos PM, Harley JD, Thiele BL, Strandness DE. Carotid-Artery Velocity Patterns in Normal and Stenotic Vessels. *Stroke* 1980;11(1):67–71. [PubMed: 7355433]
34. Nezafat R, Stuber M, Ouwerkerk R, Gharib AM, Desai MY, Pettigrew RI. B-1-insensitive T-2 preparation for improved coronary magnetic resonance angiography at 3 T. *Magnetic Resonance in Medicine* 2006;55(4):858–864. [PubMed: 16538606]
35. Chierigato A, Calzolari F, Trasforini G, Targa L, Latronico N. Normal jugular bulb oxygen saturation. *J Neurol Neurosurg Psychiatry* 2003;74(6):784–786. [PubMed: 12754351]
36. Leenders KL, Perani D, Lammertsma AA, Heather JD, Buckingham P, Healy MJR, Gibbs JM, Wise RJS, Hatazawa J, Herold S, Beaney RP, Brooks DJ, Spinks T, Rhodes C, Frackowiak RSJ, Jones T. Cerebral Blood-Flow, Blood-Volume and Oxygen Utilization -Normal Values and Effect of Age. *Brain* 1990;113:27–47. [PubMed: 2302536]
37. Raichle ME, MacLeod AM, Snyder AZ, Powers WJ, Gusnard DA, Shulman GL. A default mode of brain function. *Proc Natl Acad Sci U S A* 2001;98(2):676–682. [PubMed: 11209064]
38. Fox PT, Raichle ME, Mintun MA, Dence C. Nonoxidative Glucose Consumption During Focal Physiologic Neural Activity. *Science* 1988;241(4864):462–464. [PubMed: 3260686]
39. An HY, Lin WL. Quantitative measurements of cerebral blood oxygen saturation using magnetic resonance imaging. *Journal of Cerebral Blood Flow and Metabolism* 2000;20(8):1225–1236. [PubMed: 10950383]
40. He X, Yablonskiy DA. Quantitative BOLD: Mapping of human cerebral deoxygenated blood volume and oxygen extraction fraction: Default state. *Magnetic Resonance in Medicine* 2007;57(1):115–126. [PubMed: 17191227]

41. Fernandez-Seara MA, Techawiboonwong A, Detre JA, Wehrli FW. MR susceptometry for measuring global brain oxygen extraction. *Magnetic Resonance in Medicine* 2006;55(5):967–973. [PubMed: 16598726]
42. Chen JJ, Pike GB. Global cerebral oxidative metabolism during hypercapnia and hypocapnia in humans: implications for BOLD fMRI. *Journal of Cerebral Blood Flow and Metabolism*. 2010 in press.
43. He X, Zhu M, Yablonskiy DA. Validation of oxygen extraction fraction measurement by qBOLD technique. *Magnetic Resonance in Medicine* 2008;60(4):882–888. [PubMed: 18816808]
44. Chanarin, I.; Brozovic, M.; Tidmarsh, E.; Waters, D. *Blood and its disease*. New York: Churchill Livingstone; 1984.

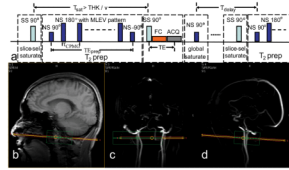


**Figure 1.**

(a) Pulse sequence diagram for measuring blood  $T_2$  in the internal jugular vein (IJV). There are 4 blocks within each TR: slice-selective (SS) saturation, non-selective (NS)  $T_2$  prep, SS excitation/acquisition, and NS saturation.  $T_{\text{sat}} = 200$  ms,  $\tau_{\text{CPMG}} = 10$  ms,  $TE_{\text{prep}} = [20, 40, 80, 160]$  ms, and  $TE = 15$  ms,  $T_{\text{delay}} = 2$  s. (b–c) Localization of IJV: (b) Anatomical scout image with sagittal view. Angiographic scout images with coronal view (c) and with sagittal view (d) are also shown. The orange line indicates the center of the imaging slice (red) perpendicular to the neck vessels in both coronal view and sagittal view. The green box is the localized shimming box that aligns with the imaging slice and is centered at the side of the largest IJV of the subjects.

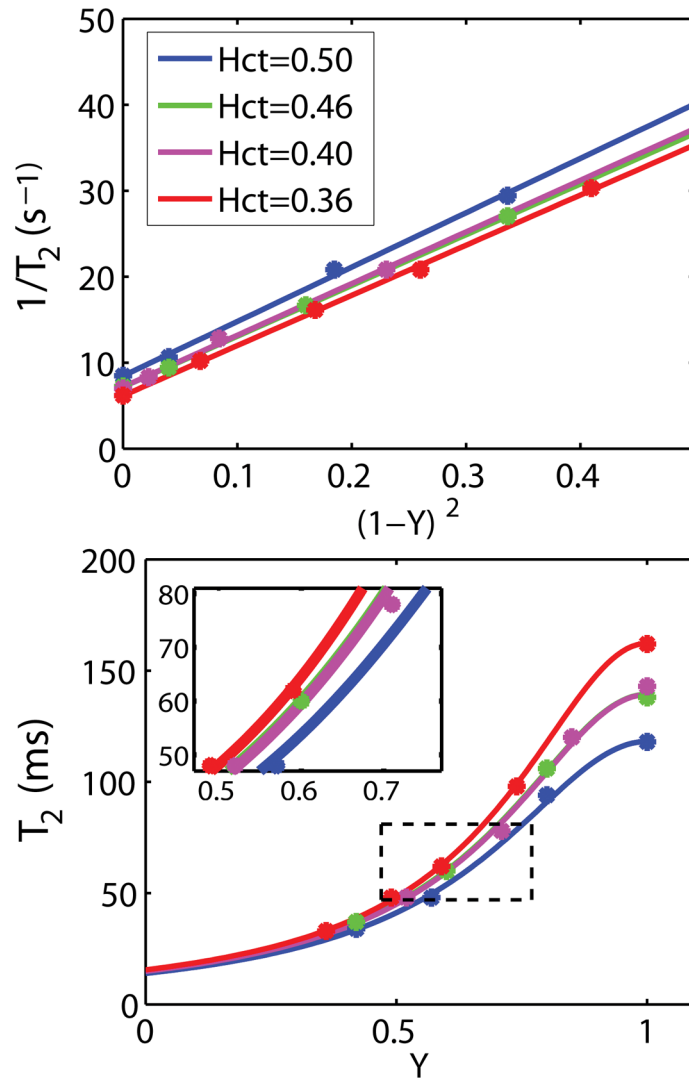


**Figure 2.**

Dependencies of the transverse relaxation rate of blood at 3T on deoxygenation (a) and oxygen saturation fraction (b). (a) Results for all four Hct values show a linear dependence (Eq. [3]) on the square of deoxygenation level,  $(1-Y)^2$  for  $\tau_{\text{CPMG}} = 10$  ms ( $R^2 > 0.99$ ). (b) The corresponding  $T_2$  vs.  $Y$  curves. The average of the Hct = 0.40 and Hct = 0.46 curves in (a) and (b) were used for the calibration curve for *in vivo* OEF estimation. The 50 to 80 ms  $T_2$  range is zoomed out to show the effect of Hct, which causes only about 4 ~ 6% error as calculated in the Results session. All fit parameters are summarized in Table 1.

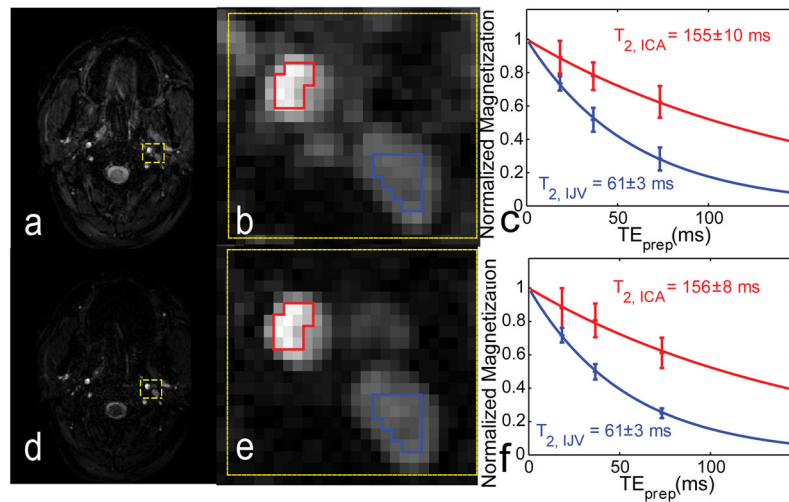


**Figure 3.**

Effect of the slice-selective pre-saturation block on image contrast and measured  $T_2$  values. The first row shows an image ( $TE_{\text{prep}} = 20$  ms) collected without saturation (a), with the zoomed-in view in the yellow box (b) and corresponding  $T_2$  curves (c) from vascular ROIs (blue: IJV; red: ICA). In the second row, SS saturation was enabled (d–f). By minimizing static tissue magnetization using SS saturation before  $T_2$  prep, identifying of ROIs around the jugular veins are substantially facilitated (d, e). This additional pulse also does not affect the  $T_2$  fitting for the flowing blood (f). The estimated  $T_2$ s fitted from the averaged ROI signals are reported with the standard error of the nonlinear fit.

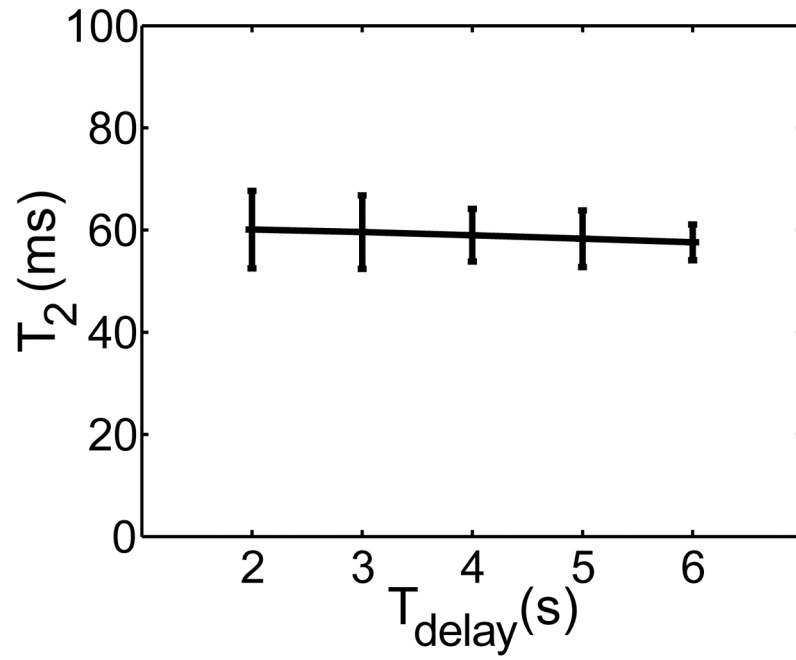


**Figure 4.** Average  $T_2$ s fitted for all subjects as a function of  $T_{\text{delay}}$ , showing excellent agreement for all delays. Error bars reflect the std across subjects. It can be seen that longer  $T_{\text{delay}}$  leads to higher SNR and less variation among subjects, with the cost of longer acquisition time.



**Table 1**

Quadratic fitting of Eq. [3] of *in vitro* blood (3T, 37°C) at  $\tau_{\text{CPMG}} = 10$  ms with four Hct values within physiology range, as well as the calculated  $T_2$  for a typical venous oxygenation level of 0.61. The standard errors of A and C are shown as the uncertainty of the fit, which are then taken into account in the uncertainty estimation of the venous  $T_2$  with  $Y=0.61$ .

Hct	A	C	$T_2$ (ms) ( $Y_v=0.61$ )
0.36	6.16±0.24	58.4±1.1	66.5±1.3
0.40	7.18±0.33	60.1±2.7	61.3±2.0
0.46	7.18±0.07	59.0±0.4	61.9±0.4
0.50	8.46±0.43	63.2±2.2	55.3±1.7

**Table 2**

Measured  $T_{2, \text{IV}}$  of 20 subjects and their individual  $Y_v$  (using Eq. [3],  $A = 7.18$ ,  $C = 59.6$ ) and corresponding OEF estimation (Eq. [4], assuming  $Y_a = 0.98$ ). The standard errors of the fitted  $T_{2, \text{IV}}$ , and their error propagations into  $Y_v$  and OEF, are shown as the uncertainty of the results for each individual.

subject	$T_{2, \text{IV}}$ (ms)	$Y_v$	OEF
female:1	68±6	0.64±0.06	0.34±0.06
2	54±2	0.56±0.03	0.42±0.03
3	67±2	0.64±0.02	0.35±0.03
4	60±3	0.60±0.04	0.39±0.04
5	72±1	0.66±0.02	0.32±0.02
6	54±1	0.56±0.02	0.42±0.02
7	70±2	0.65±0.02	0.33±0.02
8	67±2	0.64±0.02	0.35±0.03
9	67±2	0.64±0.02	0.35±0.03
10	55±2	0.57±0.03	0.42±0.03
<b>mean ± std:</b>	<b>63.4 ± 7.0</b>	<b>0.62 ± 0.04</b>	<b>0.37 ± 0.04</b>
male:1	61±3	0.61±0.04	0.38±0.04
2	68±4	0.64±0.04	0.34±0.04
3	57±3	0.58±0.04	0.41±0.04
4	54±4	0.56±0.05	0.42±0.06
5	68±4	0.64±0.04	0.34±0.04
6	55±1	0.57±0.02	0.42±0.02
7	64±2	0.62±0.03	0.36±0.03
8	66±1	0.63±0.02	0.35±0.02
9	64±2	0.62±0.03	0.36±0.03
10	57±1	0.58±0.02	0.41±0.02
<b>mean ± std:</b>	<b>61.4 ± 5.3</b>	<b>0.61 ± 0.03</b>	<b>0.38 ± 0.03</b>
female and male data combined			
<b>mean ± std:</b>	<b>62.4 ± 6.1</b>	<b>0.61 ± 0.03</b>	<b>0.37 ± 0.04</b>

**Table 3**

Comparison of determined OEF with existing literature values for normal subjects.

Modality	Reference	Measurement location	OEF: mean±std (range, n)	Measurement time (minutes)
Catheterisation	Chierigato et al., 2003 (35)	Jugular bulb	0.42 (0.29~0.54, n=12)	
PET	Leender et al., 1990 (36)	Gray Matter	0.42 (0.27~0.50, n=34)	
PET	Raichle et al., 2001 (37)	Gray/White Matter	0.40±0.09 (n=19)	
PET	Fox et al., 1988 (38)	Visual Cortex	0.36 <sup>1</sup>	
MRI 1.5T T <sub>2</sub>	Oja et al., 1999 (15)	draining veins near Visual Cortex	0.45 (0.37~0.54, n=7) <sup>2</sup>	11.0
MRI 1.5T T <sub>2</sub>	Golay et al., 2001 (16)	draining veins near Visual Cortex	0.38±0.04 (0.30~0.46, n=8)	6.0
MRI 3.0T T <sub>2</sub>	Lu et al., 2007 (19)	Sagittal Sinus	0.34±0.06 (n=24)	4.3
MRI 3.0T T <sub>2</sub>	Chen et al., 2010 (42)	IJV	0.40±0.08 <sup>3</sup> (n=10)	4.5
MRI 1.5T T <sub>2</sub> '	An et al., 2000 (39)	Gray/White Matter	0.40±0.02 (0.37~0.44, n=8)	8.5
MRI 3.0T T <sub>2</sub> '	He et al., 2007 (40)	Gray/White Matter	0.38±0.05 (0.33~0.48, n=9)	8.5
MRI 3.0T susceptibility	Fernandez-Seara et al., 2006 (41)	IJV	0.33±0.08 (n=5)	4.3
MRI 3.0T T <sub>2</sub>	this study	IJV	0.37±0.04 (0.32~0.42, n=20)	0.8

<sup>1</sup> Calculated using  $CMRO_2 = 1.5 \mu\text{mol/g/min}$ ,  $Hct = 0.41$ , and  $CBF = 0.5 \text{ ml/g/min}$ .

<sup>2</sup> Recalculated from Oja's  $T_{2V}$  values using the newly determined calibration constants by Golay et al. at 1.5T (16).

<sup>3</sup> Calculated using  $Y_V = 0.58$  and  $Y_a = 0.98$  (42).